plasma

MDPI

Article

Features of Pinch Plasma, Electron, and Ion Beams That Originated in the AECS PF-1 Plasma Focus Device

Mohamad Akel *, Sharif AL-Hawat, Muthanna Ahmad, Yamen Ballul and Soliman Shaaban

Department of Physics, Atomic Energy Commission, Damascus P.O. Box 6091, Syria; shalhawat@aecs.sy (S.A.-H.); mahmad@aecs.sy (M.A.); yballul@aecs.sy (Y.B.); sshaaban@aecs.sy (S.S.)

* Correspondence: pscientific14@aec.org.sy

Abstract: The measured current traces of alow energy AECS PF-1 plasma focus device are used for studying of the formed plasma, and the produced ion and electron beams. Anadapted version of the Lee model (RADPFV5.15FIB&REB) is applied, taking into account the fitting procedures between the measured and computed current waveforms for each shot. The experiments on AECSPF-1 were performed with three different gases—helium, nitrogen, and argon—for studying the effect of the atomic number on the properties of the generated beams. For numerical experiments using the Lee model, 36 successful shots for each gas were selected. The peak values of the total discharge current I_{peak} were 50–55 kA, the pinch currents I_{pinch}were34–36 kA, and the final pinch radius reached a minimum value of 0.03 cm for argon. The ion mean energy ranged from 35 keV (for He) to 223 keV (for Ar). The beam energy also had an extreme value of 1.34 J (0.05%E_0) for argon. The results presented the highest values of 2.4×10^{14}Wm^{-2} for the power flow density, and adamage factor of around 3.1×10^{10} Wm^{-2}s$^{0.5}$ for argon. For electron beams, the results also showed that the fluence and flux increased with the higher atomic number and reached a peak of 9.7×10^{22} m^{-2} and 5.9×10^{30} m^{-2} s^{-1} for argon, respectively. The results presented the highest values of 2.2×10^{16}Wm^{-2} for the power flow density (heat flux), and adamage factor of around 3×10^{12} Wm^{-2}s$^{0.5}$ for argon. The kinetic energy of the relativistic electrons was found to be within the range of 18–23 keV. The results show that the ion and electron beam properties (energy, flux, fluence, ion and electron numbers, current, power flow density, and damage factor) emitted from the plasma focus had wide ranges based on the operational plasma focus parameters. Thus, these results could be used for selection of the suitable plasma focus parameters for desired material processing applications.

Keywords: electron and ion beam; plasma focus; Lee model; various gases

Citation: Akel, M.; AL-Hawat, S.; Ahmad, M.; Ballul, Y.; Shaaban, S. Features of Pinch Plasma, Electron, and Ion Beams That Originated in the AECS PF-1 Plasma Focus Device. *Plasma* **2022**, *5*, 184–195. https://doi.org/10.3390/plasma5020014

Academic Editor: Eun Ha Choi

Received: 23 December 2021
Accepted: 18 March 2022
Published: 25 March 2022

1. Introduction

Many experiments and efforts have been performed on the plasma focus for multi-applications such as neutrons, X-radiation, and high energetic particle generation. Most experiments for ion beam diagnostics have been conducted with deuterium to investigate the neutron production and deuteron acceleration. It was found that the pinched plasma shape is related to the acceleration of deuterons. However, when a high atomic number gas is used as a filling gas, the plasma focus phenomena are the changes from a long column to a short hot spot [1]. The electrons produced by the plasma focus devices have been studied using different diagnostics [2–5]. The electron beam energy emitted from the NX2 device was measured and was found to be around 3.2% of the storage energy E_0 [3]. The mean electron beam current produced in a 2.2 kJ PF device operated with nitrogen was estimated to be about 13.5 kA (at 0.3 Torr) and the electron energy was ~80–110 keV [5]. The origin of electrons and ions in the plasma focus devices have been studied and discussed [6–8]. A low energy 3 kJ plasma focus device operated with neon has been utilized to study electrons, where the energy of electron was less than 200 keV [9]. The radiation from the

dense hot plasma may affect plasmadynamics, causing radiative cooling and collapse for high Z gases such as Ar, Kr, and Xe [10–12]. Experimental observations suggests Ar (Z = 18) as the transition gas, below which (Z < 18) the pinching and any radiative cooling effects proceed as a column. For heavier gases (Z > 18), the pinch is broken up into a line of radiatively collapsed dense hot spots [13]. In the plasma focus, the Faraday Cup is used to measure the ion flux, which was found to be 4.34×10^{16}–1.86×10^{17} ions/sterad for an energy range of 3–12keV [14]. The results on a Mather type 2.3 kJ PF showed that the ion current density decreased from 1.4×10^{7} Am^{-2} to 1.1×10^{7} Am^{-2} as the BPX65 diode moved from 3–9 cm [15]. In another experiment, the results showed that the average ion current density estimated for the solid anode changed with the gas pressure from 1.15×10^{7} Am^{-2} (at 0.13 mbar of nitrogen) to 0.6×10^{7} Am^{-2} (at 1.33 mbar of nitrogen) with a maximum value of 1.25×10^{7} Am^{-2} (at 0.7 mbar of nitrogen) [16]. H. Kelly et al. [17] recorded, in PF II (4.75 kJ, 30 kV), 3.2×10^{13} ions/sterad with an energy content of 0.74 J/sterad, measuring ion energies in the range of 50–1000 keV. Sohrabi et al. [18] reported a maximum ion density of about 10^{25} ions m^{-2} using the Faraday Cup method. Ion fluences of 10^{18}–10^{20} m^{-2}werefound using 300–400 ns ion nitrogen pulses [19]. M. Habibi et al. [20] found that a maximum ion flux of 6×10^{12} ions/steradian was obtained with a cylindrical anode tip that increased to 10^{13} ions/steradian for a conical anode tip. The Lee model code [21] was extended, based on the virtual plasma diode mechanism proposed by Gribkov et al. [22,23], for studying ion beams from the plasma focus [13,24–26], and later were further developed to consider the electron beams from the plasma focus [27,28]. The correlation between the plasma focus parameters and produced ion and electron beam properties could be of help to understand the plasma surface interactions and to find the optimum conditions for the desired material science applications.

So, the major aim of this work wasto investigate the influence of the atomic number on the properties of the generated beams and to provide a basis for estimating the effects of ion and electron beams emitted from the plasma focus on target materials, especially for a single capacitor with an energy of kJ plasma focus devices that dominate the research for small plasma focus groups.

2. Materials and Methods

2.1. Experimental Set up and Diagnostic Tools

The experiments were investigated using AECS PF-1 [29,30] (see Table 1) with helium, nitrogen, and argon gases at an operational optimum pressure of 0.6 ± 0.02 Torr. The electrode system consisted of a central solid cylindrical copper anode of 16 cm in length and 1.9 cm in diameter, and a cathode consisting of six copper rods arranged in a circle of 6.4 cm diameter concentric with the anode. In this work, the copper anode was modified by encapsulating pure Sn(99.99%) in the top of the anode (diameter of 1.8 cm). The anode was insulated from the cathode at the back wall using a Pyrex glass tube of 5 cm in length and 2.4 cm in diameter. To reduce the impurity effect, after every shot, the previous gas was purged and fresh gas was filled. The current in the discharge circuit and the voltage across the AECS PF-1 versus time during the plasma focus discharge were measured at the main collector plate using a Rogowski coil and an Ohmic voltage divider 1:100 probe, respectively. Four-channel digital storage oscilloscopes (TDS 3054C) with shielded connecting cables were used to record the current and voltage signals simultaneously.

Table 1. The technical parameters of AECS-PF1plasma focus device.

Operating Parameters	Description
Capacitance	25 μF
Operating charging voltage	15 kV
Stored energy (E_0)	2.8 kJ
Peak discharge current	54 kA
Inductance of circuit	1400 nH
Anode length	16 cm
Anode radius	0.95 cm
Cathode radius	3.2 cm
Rise time of the current	~10 μs
Working gases	Nitrogen, argon, and helium

2.2. The Lee Model Code Used for the Ion and Electron Beam Computation

The five-phase Lee code is a computer code simulating approximately all main phases of discharge in the plasma focus. It has a consistent energy, mass, momentum and charge. It uses a realistic power source model and assumes the validity of the Bennett relation in each small time step of the code in the equilibrium pinch phase of discharge. It includes the finite velocity of small disturbances propagation in the plasma during radial collapse and compression, taken as the acoustic/sound velocity. The code also includes the ionization effects in the plasma, the shock-wave heating model in the radial phases of discharge before stable pinch formation, the classical model of plasma column ohmic heating based on the Spitzer resistivity, the anomalous resistivity, and heating due to micro-instability development. The code also enables X-ray bremsstrahlung, and line and recombination radiation emission from the pinch column, and couples it with plasma pinch compression dynamics. The plasma self-absorption and transition from volumetric to surface emission is also included, as well as the neutron emission based on both thermonuclear and beam-target fusion models. In the Lee model, a beam of fast deuterons is produced by a vacuum diode in a thin layer close to the anode, with plasma disruptions generating the necessary high voltages. The Lee model code simulates the total current. Four model parameters are used, representing the mass swept-up factor (f_m) and the plasma current factor (f_c) for the axial phase, as well as the mass swept-up factor (f_{mr}) and the plasma current factor (f_{cr}) for the radial phases. These four model parameters are used to account for the experimentally observed mass loss and current loss in the axial and radial phases of discharge, respectively (percentages of total mass and current flowing between electrodes in axial and radial phases). After each run, the user changes one of the model parameters so as to improve the fitting of the computed to the measured current trace for the next run. This fitting procedure is done sequentially, starting with f_m and f_c while inspecting the fit of the current trace in the axial phase before the current dip, and then proceeds to f_{mr} and f_{cr} while inspecting the fit of the current dip. Additionally, static inductance L_0 and stray resistance r_0 parameters may be fine-tuned from run to run during the fitting procedure of current traces. In general, it is well known that the current signal from a plasma focus is one of the best performance indicators that can be obtained. Some of the most important information that can be derived using the Lee model, like the axial and radial phase dynamics, as well as radiation yields, are dependent on the current flow in the plasma. Moreover, once fitted, the code outputs the following realistic data: the dynamics and energy content of the phases, pinch geometry, temperatures and densities, line radiation, and neutron yields. In this article, all experimental discharges (experimental current traces) were fitted individually with simulated discharges (simulated current traces) using four model parameters, as well as L_0 and r_0 parameters.

The flux equation of the ion beam emitted from the plasma pinch is derived and inserted into the Lee model code, which is in turn used to study the ion beam properties [13,25,26]. As the beam exits the focus pinch with little divergence, the exit

beam is best characterized by the ion fluence, defined as the number per unit cross-section. During the numerical experiments, the following equation is utilized for the ion flux:

$$\text{Flux (ions m}^{-2}\text{ s}^{-1}) = 2.75 \cdot 10^{15} \cdot \frac{f_e \cdot \ln(b/r_p) \cdot I_{pinch}^2}{M^{1/2} \cdot Z_{eff}^{1/2} \cdot r_p^2 \cdot U^{1/2}} \quad (1)$$

The ion fluence (ions m^{-2}) is then computed by multiplying the flux by the pinch duration.

Here, Mis the mass number of ion; b is the cathode radius; and $f_e = 0.14$ (the fraction of energy converted from pinch inductive energy PIE into beam kinetic energy BKE), which is equivalent to an ion beam energy of 3–6% E_0. The diode voltage U is $U = 3V_{max}$, taken from the data fitting, where V_{max} is the maximum induced voltage in the axial phase. The code computes the values of effective charge Z_{eff}, pinch radius r_p, pinch duration, pinch current I_{pinch}, and U from which the ion flux is deduced, followed by fluence ions m^{-2} current density (Am^{-2}), current (A), ions per sec (ions s^{-1}), number of ions in beam (ions), power density flow (energy flux) (Wm^{-2}), energy in beam (J), and damage factor ($Wm^{-2}s^{0.5}$).

Next, for studying the electron beam characteristics generated in the pinch using the Lee model, the corresponding equations are first deduced and they are then incorporated into the code. Firstly, the electron beam flux formula is taken as $J_{eb} = n_{eb}v_{eb}$ (electrons per m^2s^1), where n_{eb} is the density number of beam electrons, which is equal to N_{eb} (total number of electrons) divided by the volume of the pinch plasma, and v_{eb} is the electron speed (all quantities are expressed in SI units, except where otherwise stated).

Then, based on the kinetic energy of the beam electrons and pinch inductive energy concepts, n_{eb} and v_{eb} are derived. The beam kinetic energy is $(1/2)N_{eb}m_e{v_{eb}}^2$, where m_e is the mass of the electron. The pinch inductive energy equals $(1/2)L_p{I_{pinch}}^2$, where $L_p = (2)(\ln[b/r_p])z_p$ is the inductance of the focus pinch, $=4 \times 10^{-7}$ Hm^{-1}, b is the cathode radius, r_p is the pinch radius, z_p is the length of the pinch, and I_{pinch} is the pinch current. As the kinetic energy is imparted by a fraction f_e of the pinch inductive energy, it can be written as follows $(1/2)N_{eb}m_e{v_{eb}}^2 = f_e\ (1/2)(2)(\ln[b/r_p])z_p{I_{pinch}}^2$.

This gives

$$n_{eb} = N_{eb}/({r_p}^2z_p) = (2\ m_e])\ (f_e)\ \{(\ln[b/r_p])/({r_p}^2)\}\ ({I_{pinch}}^2/{v_{eb}}^2) \quad (2)$$

Next, we proceed to derive v_{eb} from the accelerating voltage provided by the diode voltage U to an electron. Each electron is given as the kinetic energy of $E_e = (1/2)m_e{v_{eb}}^2$ by the diode voltage U. Thus, $(1/2)m_e{v_{eb}}^2 = eU$, where e is the electronic charge. Hence

$$v_{eb} = (2e/m_e)^{1/2}\ U^{1/2}. \quad (3)$$

Now, we take Equation (2) and combine it with Equation (3), and noting that $(2.83\ (em_e)^{1/2}]) = 1.2 \times 10^{17}$, we have the flux equation, as follows:

$$\text{Flux (electrons m}^{-2}\text{s}^{-1}) = J_{eb} = 1.2 \times 10^{17}\ (f_e)\{(\ln[b/r_p])/({r_p}^2)\}({I_{pinch}}^2)/U^{1/2} \quad (4)$$

The fluence is the flux multiplied by the pulse duration.

Thus:

$$\text{Fluence (electrons m}^{-2}) = 1.2 \times 10^{17}\ (f_e)\{(\ln[b/r_p])/({r_p}^2)\}({I_{pinch}}^2)/U^{1/2} \quad (5)$$

where f_e~0.14 for the energy of electron beam = 4% E_0 for cases when the pinch inductive energy holds 20–40% of E_0, as observed for low inductance PF [3]. From the above-mentioned equations, it is noticed that the electron flux and fluence is $(m_p/m_e)^{1/2}$~43 of the deuteron beam flux and fluence, where m_p is the mass of the proton. However, the experimental observations by the authors over the years show that the electron beam leaves a very fine footprint on a per shot basis, with a diameter of the order of 0.1 mm when the

ion beam is of the order of 1mm for a plasma focus with a radius of the order of 1 cm. These experimental observations seem consistent with a necessary assumption that the electron beam current be set to be approximately equal to the ion beam current. To implement this assumption in the code, the radius of the electron beam is taken as $(1/43)^{0.5}$ times the radius of the ion beam (or the radius of the pinch). The kinetic energy of the relativistic electrons is estimated by $E_{rel} = m_e c^2(\gamma - 1)$, where γ is the relativity factor $[(1/(1 - v_{eb}{}^2/c^2)^{1/2})]$, c is the light speed ($c = 3 \times 10^8 m/s$), and $m_e c^2$ is the rest mass energy of an electron ~511 keV. Once the flux is determined, the following quantities are also computed: energy flux or power density flow (Wm^{-2}), power flow (W), current density (Am^{-2}), current (A), fluence electrons m^{-2}, energy fluence ($J\ m^{-2}$), number of electrons in beam (electrons), energy in beam (J), and damage factor ($Wm^{-2}s^{0.5}$).

3. Results and Discussion

3.1. Fitting Procedures of the Current Waveforms

The measurements of the current and voltage waveforms on AECS PF-1 were investigated with three different gases—He, N_2, and Ar—at an optimum pressure of around 0.6 Torr. The considered current and voltage signals were recorded during the deposition process of tin (Sn) on the silicon substrate located at the different positions from the anode tip. Thirty-six successful shots were selected for each gas, as the plasma focus devices have a variable performance from shot-to-shot even for the same operational parameters, likely due to the random changes in the conditions of the electrodes. In this work, the measured current traces were used to compute the plasma focus parameters, and ion and electron beam properties emitted from AECS PF-1 operated with He, N_2, and Ar using the Lee model code (version: RADPFV5.15FIB&REB). The fitting procedures using the Lee model [31,32] were investigated for each meaured current step by step.

For this purpose, the Lee model code was configured as AECS PF-1 (Figure 1a,b) using the following parameters as an example:

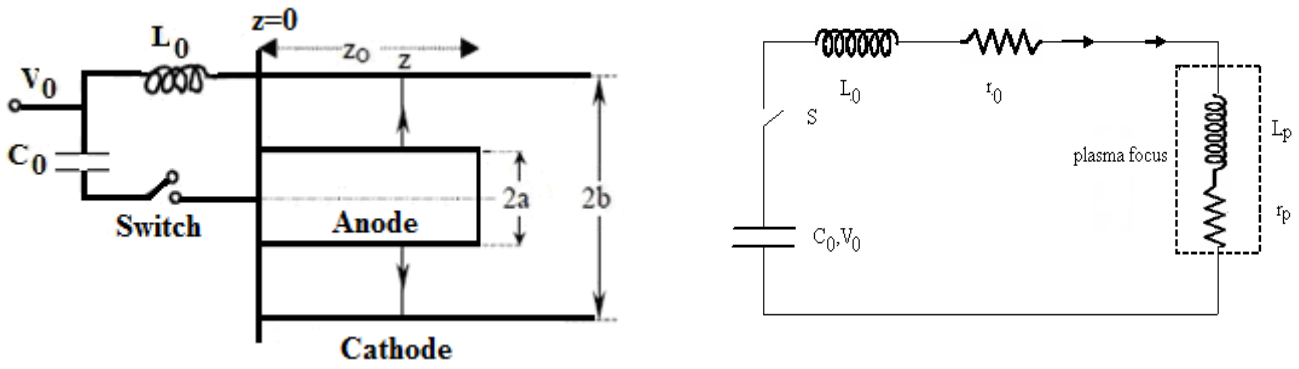

(**a**) (**b**)

Figure 1. (**a**) The major parts of plasma focus device. (**b**) Equivalent electrical circuit of the plasma focus device, where L_p and r_p are the inductance and resistance of the plasma, respectively.

Bank: L_0 = 1430 nH, C_0 = 25 μF, r_0 = 50 mΩ;
Tube: b = 3.2 cm, a = 0.95 cm, z_0 = 16 cm;
Operational: V_0 = 15 kV, p_0 = 0.6 Torr for helium gas;

where L_0, C_0, b, a, z_0, V_0, and p_0 are the static inductance (nominal), storage capacitance, cathode radius, anode radius, anode length, operating voltage, and initial pressure, respectively. The measured wave shape of the current was then used as the basis to fit the computed current. The four model parameters derived from the fitting were the axial phase mass swept-up factor f_m = 0.15, corresponding plasma current factor f_c = 0.7, the radial phase mass swept-up factor f_{mr} = 0.2, and corresponding current factor f_{cr} = 0.7. Figure 2 shows the measured and computed waveforms of the current and voltage in the AECS PF-1 plasma focus device at p_0 = 0.6 Torr of helium. The fitting seemed to be good.

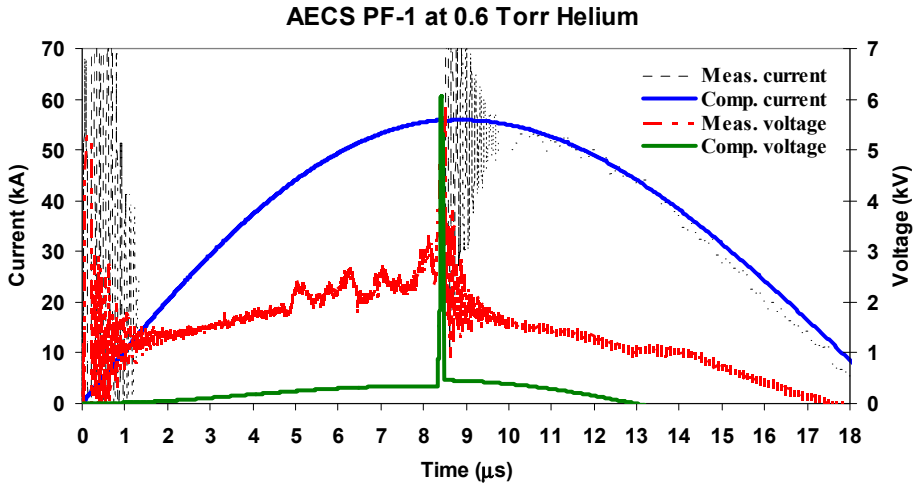

Figure 2. The measured and computed waveforms of the current and voltage in the AECS PF-1 plasma focus device at p_0 = 0.6 Torrofhelium.

Another example for the fitting procedures is illustrated in Figure 3 for the AECS PF-1 device operated with argon gas. The obtained fitting parameters wereas follows:

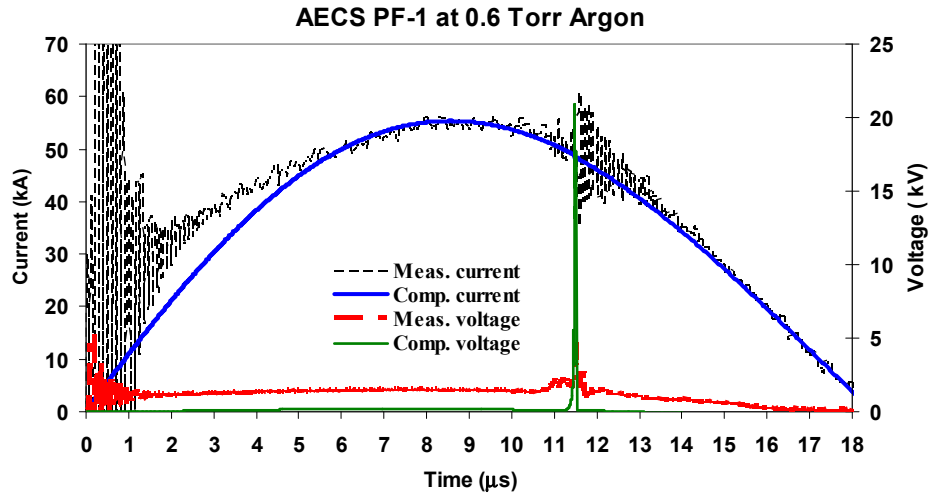

Figure 3. The measured and computed waveforms of the current and voltage in the AECS PF-1 plasma focus device at p_0 = 0.6 Torr of argon.

Bank: L_0 = 1350 nH, C_0 = 25 μF, r_0 = 46 mΩ;
Tube: b = 3.2 cm, a = 0.95 cm, z_0 = 16 cm;
Operational: V_0 = 15 kV, p_0 = 0.6 Torr for argon gas,
The four model parameters derived from the fitting were f_m = 0.09, f_c = 0.7, f_{mr} = 0.15, and f_{cr} = 0.7.

Furthermore, Figure 4 illustrates the measured focusing time using AECS PF-1 at 0.6 Torr for the three studied gases.

In the same manner, applying the adapted version of the Lee model (RADPFV5.15FIB& REB) on the plasma focus device AECS-PF1 (for He, N_2, and Ar) and taking into account the fitting procedures, the pinch plasma parameters and the properties of the electron and ion beams were determined for each shot.

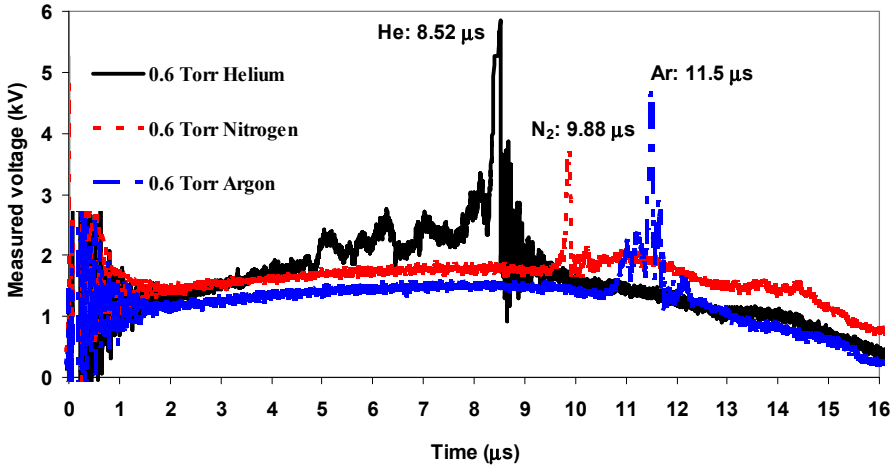

Figure 4. The focusing time in AECS PF-1 plasma focus device at p_0 = 0.6 Torr for He, N_2 and Ar gases.

3.2. Plasma Parameters Generated in the AECS PF-1 Device

In this study, 36 successful discharges performed on AECS PF-1 were selected for each operational gas, and the demonstrated results represent the mean values of the considered parameters. The plasma parameters generated in AECS PF-1 are presented in Table 2 for the three studied gases. The peak values of the total discharge current I_{peak} were 50–55 kA, the pinch currents I_{pinch} were 34–36 kA, the final pinch radius was 0.13 cm for He and it reached a minimum value of 0.03 cm for argon, the pinch length was around 1.4 cm for He and N_2 with the highest value (1.65 cm) for argon, and the pinch duration ranged from 11 to 17 ns. The maximum voltage induced by the radially collapsing current sheet V_{max} was 5.7 kV, 6 kV, and 22 kV for He, N_2, and Ar, respectively. The plasma temperature ranged from 105 eV for N_2 to the peak value of 350 eV for He. Moreover, the various speeds were calculated to be as follows for helium: The peak axial speed was V_a = 4.5 cm/µs, the shock speed (on-axis) was V_s = 24 cm/µs, and the peak radial piston speed was V_p = 16.5 cm/µs. For nitrogen, V_a = 2.5 cm/µs, V_s = 14 cm/µs, and V_p = 10 cm/µs, and the lowest speeds were for argon, V_a = 2 cm/µs, V_s = 11 cm/µs, and V_p = 9 cm/µs. The argon plasma focus had a maximum plasma density of 9×10^{23} m^{-3}.

Table 2. Average plasma focus parameters of the AECS PF-1 device at 0.6 Torr during the experiments.

AECS PF-1	He	N_2	Ar
	Average of 36 Shots	**Average of 36 Shots**	**Average of 36 Shots**
Peak current I_{peak} (kA)	50	53	55
Pinch current I_{pinch} (kA)	34	36	34
Plasma temperature T_e, (eV)	350	105	126
pinch radius r_p (cm)	0.13	0.09	0.03
Length of the pinch z_p (cm)	1.4	1.35	1.65
Pinch duration τ (ns)	11.2	13.8	17
Induced voltage V_{max} (kV)	5.7	6	21.7
Plasma density N_i ($\times10^{23}$ m^{-3})	0.7	2.3	9.1
The peak axial speed V_a (cm/µs)	4.5	2.5	2.1
The shock speed V_s (cm/µs)	24	14.4	11.4
The peak radial piston speed V_p (cm/µs)	16.5	10.2	9

3.3. Ion Beam Properties of the AECS PF-1 Device

The application of a dense plasma focus device for various material processing utilizes high energy ions. The characterization of these ions is very important, not only for understanding the mechanism of the production of high-energy ions, but also for their applications in different fields, including plasma processing (ion implantation, surface modification, thermal surface treatment, ion assisted coating, device fabrication, thin film deposition, etc.). So, the RADPFV5.15FIB&REB code was used to study the ion beam generated in the AECS PF-1 device using the fitting procedures mentioned above for each plasma focus shot. As an example, Figures 5 and 6 present the ion energy flux and the damage factor for 36 shots.

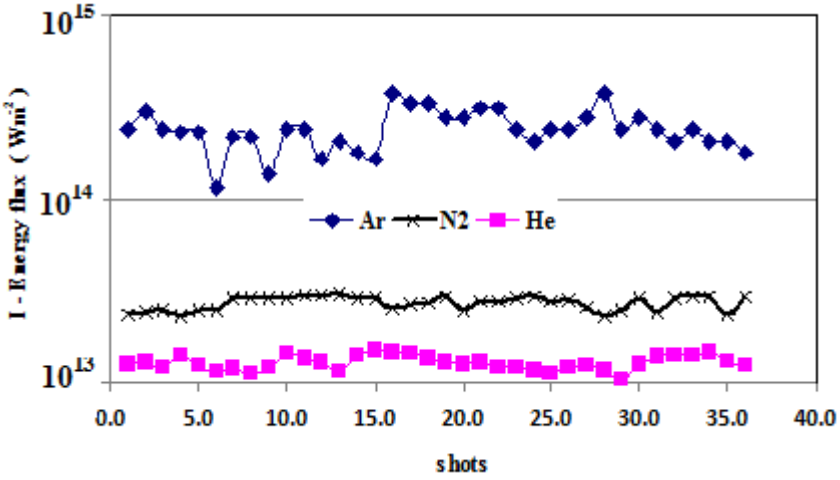

Figure 5. AECS PF-1 ion energy flux for 36 shots at 0.6 Torr for He, N_2, and Ar gases.

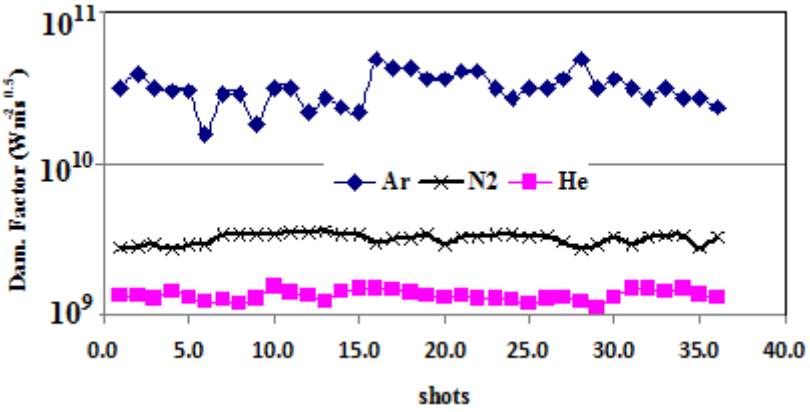

Figure 6. AECS PF-1 damage factor for 36 shots at 0.6 Torr for He, N_2, and Ar gases.

For the comparison study, the mean values of the considered parameters are illustrated in Table 3. It was noticed that the ion mean energy ranged from 35 keV (for He) to 223 keV (for Ar). The very high ion mean energy (computed by $U \times Z_{eff}$) value of Ar was due to the large diode plasma voltage and high effective charge state Z_{eff}. The results indicate that the ion fluence ranged from 0.2×10^{20} ions m^{-2} for nitrogen gas, increasing to the heavier gases until a value of 1.1×10^{20} ions $m^{-2}$was achieved for Ar. The ion number ranged from 3.8×10^{13} (for Ar) to 1.3×10^{14} (for He). The beam energy also had an extreme value of 1.34 J ($0.05\%E_0$) for argon. The results presented the highest values of 2.4×10^{14} Wm^{-2} for the power flow density (heat flux), and adamage factor of around 3.1×10^{10} $Wm^{-2}s^{0.5}$ for argon. The large values for argon gas were due to the very small radius ratios of the pinch columns due to the radiative collapse. Plasma focus devices have three typical regimes of influence of ion and plasma beams upon a target material

placed downstream of the pinch [23]: (i) "implantation mode" of irradiation when the power flow density of the streams is 10^9–10^{11} Wm^{-2}, (ii) screening of the surface by a secondary plasma cloud in the so-called "detachment mode" ($\approx 10^{11}$–10^{12} Wm^{-2}), and (iii) strong damage with the absence of implantation in the "explosive destruction mode" ($\approx 10^{12}$–10^{14} Wm^{-2}). The numerical experiments on the AECS PF-1 device showed that the power flow density ranged from10^{13}–10^{14} Wm^{-2} for the studied gases. So, based on the obtained power flow densities, it couldbe said that the explosive destruction mode was dominant for the experimental conditions used. With this method, ion beam and fast plasma stream parameters could be computed for any Mather-type plasma focus operating with different gases.

Table 3. Average ion beam characteristics of the AECS PF-1 device at 0.6 Torr for N_2, Ar, and He.

AECS PF-1	He	N_2	Ar
	Average of 36 Shots	**Average of 36 Shots**	**Average of 36 Shots**
Ion beam(IB) fluence ($\times 10^{20}$ m^{-2})	0.3	0.22	1.1
Ion flux ($\times 10^{27}$ m^{-2} s^{-1})	2.4	1.6	6.6
Ion energy (keV)	35	105	223
En fluence ($\times 10^6$ J m^{-2})	0.14	0.37	4.1
En flux ($\times 10^{14}$ Wm^{-2})	0.13	0.27	2.4
Ion number ($\times 10^{13}$)	13	6.2	3.8
IB energy (J)	0.75	1.05	1.34
IB energy (%E_0)	0.025	0.04	0.05
IB current (kA)	3.8	4.1	3.6
IB current (%I_{peak})	8	7.75	6.5
IB curr. den. ($\times 10^{10}$ A m^{-2})	0.1	0.15	1.1
Damage factor ($\times 10^{10}$ $Wm^{-2}s^{0.5}$)	0.14	0.32	3.1

3.4. Electron Beam Properties of the AECS PF-1 Device

The modified Lee (RADPFV5.15FIB&REB) code also provides information about the electron beam that originates in the pinch plasma of the AECS PF-1 device. For example, Figures 7 and 8 present the electron beam flux and the electron energy for 36 shots.

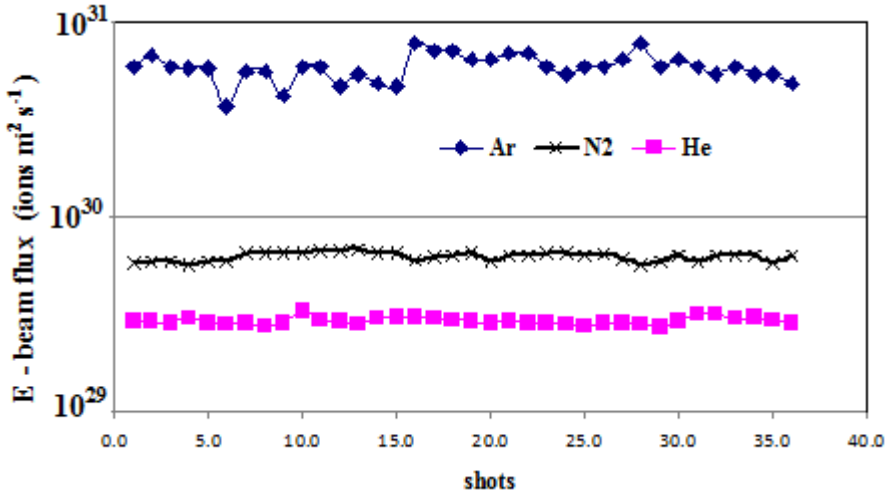

Figure 7. AECS PF-1 electron beam flux for 36 shots at 0.6 Torr for He, N_2, and Ar gases.

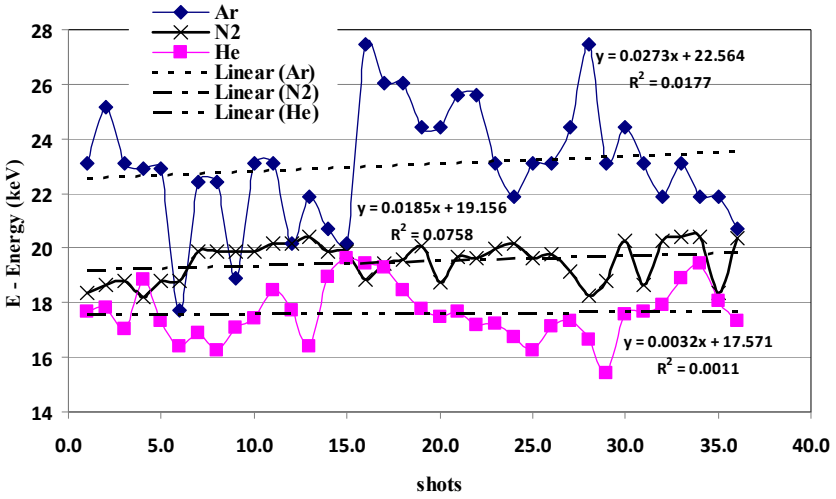

Figure 8. Electron energy for 36 shots of AECS PF-1 at 0.6 Torr for He, N_2, and Ar gases.

The mean values of the generated electron beam features for each gas are shown in Table 4. It shows that the fluence and flux increased with the higher atomic number, and reached a peak of 9.7×10^{22} m^{-2} and 5.9×10^{30} electrons m^{-2} s^{-1} for argon, respectively. The electron number ranged from 2.7×10^{14} (for He) to 5.5×10^{14} (for Ar). The beam energy also had a value of 2 J (0.072%E_0) for argon, 1.25 J (0.045%E_0) for nitrogen, and 0.78 J (0.03%E_0) for helium. The results presented the highest values of $2.2 \times 10^{16}$$Wm^{-2}$ for the power flow density (heat flux), and adamage factor of around $3 \times 10^{12}$$Wm^{-2}s^{0.5}$at 0.6 Torr of argon due tothe radiatively enhanced compression. The electron currents had values from 3.9 kA for helium (8.12% I_{peak}) to 5.2 kA (9.4% of I_{peak}) for argon. The kinetic energy of the relativistic electrons was found to be within the range of 18–23 keV.

Table 4. Average electron beam characteristics of the AECSPF-1 device.

AECS PF-1	He	N_2	Ar
	Average of 36 Shots	**Average of 36 Shots**	**Average of 36 Shots**
Electron beam (EB) fluence ($\times 10^{22}$ m^{-2})	0.35	0.86	9.7
EB flux ($\times 10^{30}$ m^{-2} s^{-1})	0.3	0.62	5.9
The kinetic energy of the relativistic electrons E_{rel} (keV)	18	19.5	23.1
Energy fluence ($\times 10^{8}$ J m^{-2})	0.1	0.27	3.73
Energy flux (Heat flux) ($\times 10^{16}$ Wm^{-2})	0.09	0.2	2.2
Electron number ($\times 10^{14}$)	2.7	3.99	5.48
EB energy (J)	0.78	1.25	2
EB energy (%E_0Stored energy)	0.028	0.045	0.072
EB current (kA)	3.9	4.6	5.2
EB current (%I_{peak})	8.12	8.78	9.36
EB curr. den. ($\times 10^{11}$ A m^{-2})	0.47	1	9.4
Damage factor ($\times 10^{12}$ Wm^{-2} $s^{0.5}$)	0.1	2.3	2.87

4. Conclusions

Measurements of the current and voltage waveforms are achieved on the low energy AECS PF-1 plasma focus device with three gases (He, N_2, and Ar) around the operational pressure (~0.6 Torr) during the experiments aimed at investigating tin (Sn) deposition on

the silicon substrate under various conditions. The Lee model is adapted to the version of RADPFV5.15FIB&REB for studying theformed plasma, as well as the produced ion and electron beams, in one run. The fitting procedures between the measured and computed current waveforms are applied for each shot. Then, numerical experiments are carried out using the Lee model on 36 successful shots for each gas.

The pinch plasma parameters are found to be I_{peak} of ~50–55 kA, I_{pinch} of ~34–36 kA, final pinch radius of ~0.03–0.13 cm, and a pinch duration of ~11–17 ns. The plasma temperature has a peak value of 350 eV for He. The argon plasma focus has a maximum plasma density of 9×10^{23} m^{-3}.

It is noticed that the beam ion mean energy ranges from 35 keV (for He) to 223 keV (for Ar), due to the higher diode plasma voltage and Z_{eff}. The ion fluence ranges from 0.2×10^{20} ions m^{-2} for nitrogen gas, increasing for the heavier gases until a value of 1.1×10^{20} ions m^{-2} is achieved for Ar. The beam energy also has an extreme value of 1.34 J (0.05%E_0) for argon. The highest values of 2.4×10^{14} Wm^{-2} for the power flow density and adamage factor of around 3.1×10^{10} $Wm^{-2}s^{0.5}$ for argon can be attributed to the very small radius ratios (r_p/a) of the pinch columns due to radiative collapse. The power flow density values of an order of 10^{13}–10^{14} Wm^{-2} for the studied gases indicate that the explosive destruction mode is dominant for the experimental conditions used.

The fluence and flux values of the generated electron beams increase with the higher atomic number and reach a peak of 9.7×10^{22} $m^{-2}$and 5.9×10^{30} m^{-2} s^{-1} for argon, respectively. The electron number ranges from 2.7×10^{14} (for He) to 5.5×10^{14} (for Ar). The beam energy also has a value of 2 J (0.072%E_0) for argon, 1.25 J (0.045%E_0) for nitrogen, and 0.78 J (0.03%E_0) for helium. The highest values of 2.2×10^{16} Wm^{-2} and 3×10^{12} $Wm^{-2}s^{0.5}$ for argon are a result of the radiative collapse effect. The electron currents have values from 3.9 kA for helium (8.12% I_{peak}) to 5.2 kA (9.4% of I_{peak}) for argon.

Finally, it is worth mentioning that due to the high inductance (1400 nH) and the relatively low peak current (54 kA) of the (2.8 kJ) AECS PF-1 device, the estimations of the ion and electron properties are comparable, but lower than the earlier published values on (20 nH, 400 kA, 2.7 kJ) NX2 [13], (110 nH, 200 kA, 3.4 kJ) INTI PF [26,28] low energy plasma focus devices with a lower inductance and higher maximum current.

Author Contributions: Conceptualization, M.A. (Mohamad Akel); Methodology, M.A. (Mohamad Akel); Software, M.A. (Mohamad Akel), Y.B. and S.S.; Validation, S.A.-H.; formal analysis, M.A. (Mohamad Akel); Investigation, S.A.-H. and M.A. (Muthanna Ahmad); resources, M.A. (Mohamad Akel); Writing—Original draft preparation, M.A. (Mohamad Akel); Writing—Reviewing and Editing, S.A.-H. and M.A. (Muthanna Ahmad). All authors have read and agreed to the published version of the manuscript.

Funding: This research received no external funding.

Institutional Review Board Statement: This study did not require ethical approval.

Acknowledgments: The authors would like to thank the Director General of AECS for the encouragement and permanent support. This work was carried out within the framework of IAEA Research Contract No. SYR-23218 of CRP F43024 (Atomic Data for Vapour Shielding in Fusion Devices).

Conflicts of Interest: The authors declare no conflict of interest.

References

1. Auluck, S.; Kubes, P.; Paduch, M.; Sadowski, M.J.; Krauz, V.I.; Lee, S.; Soto, L.; Scholz, M.; Miklaszewski, R.; Schmidt, H.; et al. Update on the Scientific Status of the Plasma Focus. *Plasma* **2021**, *4*, 450–669. [CrossRef]
2. Hirano, K.; Kaneko, I.; Shimoda, K.; Yamamoto, T. A method for measuring electron energy distribution in a plasma focus. *Jpn. J. Appl. Phys.* **1990**, *29*, 1182–1188. [CrossRef]
3. Zhang, T.; Lin, J.; Patran, A.; Wong, D.; Hassan, S.M.; Mahmood, S.; White, T.; Tan, T.L.; Springham, S.V.; Lee, S.; et al. Optimization of a plasma focus device as an electron beam source for thin film deposition. *Plasma Sources Sci. Technol.* **2007**, *16*, 250–256. [CrossRef]
4. Khan, M.Z.; Lim, L.K.; Yap, S.L.; Wong, C.S. Imperative function of electron beams in low-energy plasma focus device. *Pramana J. Phys.* **2015**, *85*, 1–3. [CrossRef]

5. Khan, M.Z.; Ling, Y.S.; Yaqoob, I.; Kumar, N.N.; Kuang, L.L.; San, W.C. Effects of different mineral admixtures on the properties of fresh concrete. *Scient. World J.* **2014**, *2014*, 240729. [CrossRef] [PubMed]
6. Tartari, A.; Da, A.R.; Bonifazzi, C.; Marziani, M. Formation of Nano-Crystalline Phase in Hydrogenated Amorphous Silicon Thin Film by Plasma Focus Ion Beam Irradiation. *Nucl. Instrum. Methods Phys. Res. B* **2004**, *213*, 206–209. [CrossRef]
7. Jakubowski, L.; Sadowski, M.J. Hot-spots in plasma-focus discharges as intense sources of different radiation pulses. *Braz. J. Phys.* **2002**, *32*, 187–192. [CrossRef]
8. Pouzo, J.; Acuna, H.; Milanese, M.; Moroso, R. Relativistic electron beams detection in a dense plasma focus. *Eur. Phys. J. D* **2002**, *21*, 97–100. [CrossRef]
9. Patran, A.; Stoenescu, D.; Rawat, R.S.; Springham, S.V.; Tan, T.L.; Tan, L.C.; Rafique, M.S.; Lee, P.; Lee, S. A magnetic electron analyzer for plasma focus electron energy distribution studies. *J. Fusion Energy* **2006**, *25*, 57–66. [CrossRef]
10. Lee, S.; Saw, S.H.; Ali, J. Numerical experiments on radiative cooling and collapse in plasma focus operated in krypton. *J. Fusion Energy* **2013**, *32*, 42–49. [CrossRef]
11. Akel, M.; Lee, S. Radiative Collapse in Plasma Focus Operated with Heavy Noble Gases. *J. Fusion Energy* **2013**, *32*, 111–116. [CrossRef]
12. Akel, M.; Lee, S.; Saw, S.H. Numerical Experiments in Plasma Focus Operated in Various Gases. *IEEE Trans. Plasma Sci.* **2012**, *40*, 3290–3297. [CrossRef]
13. Lee, S.; Saw, S.H. Plasma focus ion beam fluence and flux—For various gases. *Phys. Plasmas* **2013**, *20*, 062702. [CrossRef]
14. Tariq, H.A.R.; Khan, I.A.; Ikhlaq, U.; Hussnain, A. Variation of ion energy flux with increasing working gas pressures using faraday cup in plasma focus device. *J. Nat. Sci. Math.* **2008**, *48*, 65–72.
15. Hassan, M.; Qayyum, A.; Ahmad, R.; Murtaza, G.; Zakaullah, M. Nitriding of titanium by using an ion beam delivered by a plasma focus. *J. Phys. D Appl. Phys.* **2007**, *40*, 769. [CrossRef]
16. Mohanty, S.R.; Neog, N.K.; Bhuyan, H.; Rout, R.K.; Rawat, R.S.; Lee, P. Effect of anode designs on ion emission characteristics of a plasma focus device. *Jpn. J. Appl. Phys.* **2007**, *46*, 3039. [CrossRef]
17. Kelly, H.; Lepone, A.; Marquez, A.; Sadowski, M.J.; Baranowski, J.; Skladnik-Sadowska, E. Analysis of the nitrogen ion beam generated in a low-energy plasma focus device by a Faraday cup operating in the secondary electron emission mode. *IEEE Trans. Plasma Sci.* **1998**, *26*, 113. [CrossRef]
18. Sohrabi, M.; Habibi, M.; Yousefi, H.R.; Roshani, G.H. Angular Distribution Analysis of Nitrogen Ions in a Low Energy Dense Plasma Focus Device. *Contrib. Plasma Phys.* **2013**, *53*, 3. [CrossRef]
19. Feugeas, J.N.; Sanchez, G.; De Gonzalez, C.; Hermida, J.D.; Scordia, G. Pulsed ion implantation of nitrogen in pure titanium. Rad. *Rad. Eff. Defects Solids* **1993**, *25*, 1.
20. Habibi, M. Angular distribution of ion beam emitted from a 3.5 kJ plasma focus device using different shapes of anodes. *Phys. Lett. A* **2016**, *380*, 439–443. [CrossRef]
21. Lee, S. Radiative Dense Plasma Focus Computation Package: RADPF. Available online: https://www.plasmafocus.net (accessed on 13 December 2021).
22. Gribkov, V.A.; Banaszak, A.; Bienkowska, B.; Dubrovsky, A.V.; Ivanova-Stanik, I.; Jakubowski, L.; Karpinski, L.; Miklaszewski, R.A.; Paduch, M.; Sadowski, M.J.; et al. Plasma dynamics in the PF-1000 device under full-scale energy storage: II. Fast electron and ion characteristics versus neutron emission parameters and gun optimization perspectives. *J. Phys. D Appl. Phys.* **2007**, *40*, 3592–3607. [CrossRef]
23. Pimenov, V.N.; Elena, V.; Demina, S.A.; Maslyaev, L.; Ivanov, I.; Vladimir, A.; Gribkov, A.V.; Dubrovsky, Ü.; Ugaste, T.; Laas, M.S.; et al. Damage and modification of materials produced by pulsed ion and plasma streams in Dense Plasma Focus device. *Nukleonika* **2008**, *53*, 111–121.
24. Lee, S.; Saw, S.H. Plasma focus ion beam fluence and flux—Scaling with stored energy. *Phys. Plasmas* **2012**, *19*, 112703. [CrossRef]
25. Akel, M.S.; Salo, A.; Saw, S.H.; Lee, S. Properties of Ion Beams Generated by Nitrogen Plasma Focus. *J. FusionEnergy* **2014**, *33*, 189–197. [CrossRef]
26. Akel, M.S.; Salo, A.; Saw, S.H.; Lee, S. Ion Beam Features Produced by Two Plasma Focus Machines Operated with Different Gases. *IEEE Trans. Plasma Sci.* **2014**, *42*, 2202–2206. [CrossRef]
27. Akel, M.S.; Salo, A.; Saw, S.H.; Lee, S. Electron Beam Properties Emitted From Deuterium Plasma Focus: Scaling Laws. *IEEE Trans. Plasma Sci.* **2017**, *45*, 2303–2307. [CrossRef]
28. Akel, M.; AL-Hawat, S.; Lee, S.; Saw, S.H. Characterization of electron beams emitted from dense plasma focus machines using argon, neon and nitrogen. *Mod. Phys. Lett. B* **2018**, *32*, 1850397. [CrossRef]
29. Al-Hawat, S. Axial velocity measurement of current sheath in a plasma focus device using a magnetic probe. *IEEE Trans. Plasma Sci.* **2004**, *32*, 764–769. [CrossRef]
30. Al-Hawat, S.; Soukieh, M.; Abou Kharoub, M.; Al-Sadat, W. Using Mather-type plasma focus device for surface modification of AISI304 steel. *Vacuum* **2010**, *84*, 907. [CrossRef]
31. Al-Hawat, S.; Akel, M.; Saw, S.H.; Lee, S. Model parameters vs. gas pressure in two different plasma focus devices operated in Argon and Neon. *J. Fusion Energy* **2012**, *31*, 13–20. [CrossRef]
32. Lee, S. Plasma focus radiative model: Review of the Lee model code. *J. Fusion Energy* **2014**, *33*, 319–335. [CrossRef]